Front. Chem. China 2011, 6(3): 206–212
DOI 10.1007/s11458-011-0249-2

RESEARCH ARTICLE

Thin films of α-Fe_2O_3 nanoparticles using as nonmetallic SERS-active nanosensors for sub-micromolar detection

Xiaoqi FU (✉)[1,2], Shuang WANG[2], Qian ZHAO[2], Tingshun JIANG[2] and Hengbo YIN[2]

A new kind of nonmetallic nanosensors based on surface-enhanced Raman spectroscopy (SERS) have been successfully prepared by the assembly of α-Fe_2O_3 nanoparticles (NPs) onto clean quartz surface via the cross-linker of hexamethylene diisocyanate (HDI). The resultant substrates have been characterized by electron micrographs, which show that the α-Fe_2O_3 NPs distribute on the modified surface uniformly with a monolayer or sub-monolayer structure. 4-mercaptopyridine (4-Mpy) and 2-mercaptobenzothiazole (2-MBT) molecules have been used as SERS probes to estimate the detection efficiency of the α-Fe_2O_3 thin films. The SERS experiments show that it is possible to record high quality SERS spectra from probe molecules on the α-Fe_2O_3 thin films at sub-micromolar ($< 10^{-6}$ mol/L) concentration. These results indicate that the highly ordered, uniformly roughed, highly sensitive and low-cost α-Fe_2O_3 thin films are excellent candidates for nonmetallic SERS-active nanosensors.

Keywords nanosensors, SERS, α-Fe_2O_3 nanoparticles, thin film

1 Introduction

Raman spectroscopy is an important non-destructive tool for obtaining information about the structure and properties of molecules from their vibrational transitions. Although the weak intensity of the Raman scattered light and the appearance of fluorescence limit the application of normal Raman spectroscopy, the use of surface-enhanced Raman spectroscopy (SERS) is able to overcome these disadvantages and extend its application greatly. In comparison with fluorescence spectroscopy, SERS has a very narrow bandwidth of a typical Raman band (< 1 nm), while the fluorescent bands can be as high as 50 nm in width [1]. Furthermore, unlike infrared spectroscopy, SERS has the advantages of application in aqueous media and the high sensitivity for trace level detection [2]. The distinct advantages of SERS, such as low detection limit, real-time response, both qualitative and quantitative analysis capabilities, high degree of specificity and simultaneous multi-component detection, enable it to be one of the most effective analytical trace methods [3]. Therefore, many SERS-active substrates, such as nanostructured metals (Ag, Au and Cu), have been used as nanosensors for trace detection of dyes, biomaterial and other molecular species [4,5].

As we know, it is important that the optical properties of the substrate should be designed to fully maximize SERS intensities to lower the analytical limit of detection. Thus, it is essential to systematically control the distribution of nanoparticales (NPs), such as the physics dimensions, particles diameter and spacing, to optimize SERS enhancements. Among these robust SERS substrates in use today, the assembly of metal NPs to ordered structures was especially important due to their properties of high sensitivity, reproducibility, uniform roughness, easy fabrication and long time stability [6,7]. Naton groups [6,8] and Cotton groups [9] have respectively assembled metal NPs (Au, Ag) on to quartz or glass surfaces modified with organosilane such as alkylaminosilanes, alkylcyanosilane and alkylaminosilane. In 1996, Ulman [10] systematically introduced the formation of self-assembled monolayers. Nevertheless, these SERS-active nanosensors have been restricted primarily to noble metals (Ag [4,11], Au [12,13], Cu [14], Pt [15], Pd [16]). Little work about SERS signals from molecules adsorbed on metal oxide NPs thin films has been reported, and one predominant reason is that metal oxide NPs can hardly be bound to the modified surface firmly through covalent bonds to the functional groups such as NH_2, CN and SH. However, metal oxides have many novel electric, chemical, optical and magnetic properties, compared to these above metals. These metal oxides are fundamental to the development of smart and functional materials, devices and systems [17,18]. Another important advantage is that they cost much lower than noble metals. Therefore, exploiting low-cost SERS-active nonmetallic nanosensors with excellent performance remains an important task in this field.

Although SERS signals from molecules on the surfaces of the randomly arranged oxides such as ZnO [19], NiO [20],

Received August 20, 2011; accepted August 26, 2011
1. School of Material Science and Engineering, Jiangsu University, Zhenjiang 212013, China
2. School of Chemistry and Chemical Engineering, Jiangsu University, Zhenjiang 212013, China
E-mail: xfu@ujs.edu.cn

Cu_2O [21], PbS [22] and TiO_2 [23] have been observed, the Raman enhancement factors were usually on the order of 10 to 100, which are much less than the most frequently cited value (10^5–10^6) for molecules absorbed on nanostructured metal surfaces. In this article, enhancements of up to 10^4 in the Raman signal have been obtained from probe molecules adsorbed on surfaces of oxide nanosensors (α-Fe_2O_3 thin films), which is capable for the application in sub-micromolar ($< 10^{-6}$ mol/L) detection. The nanosensors are fabricated through a new and simple method by the assembly of dispersed α-Fe_2O_3 NPs onto the surface of quartz slides modified with hexamethylene diisocyanate (HDI). With the nanosensors, trace quantities of Raman responded species can be detected, and their adsorption behaviors on the surface such as the interaction and orientation of molecules with the surface can be conferred. We have also changed the size of α-Fe_2O_3 particles for the fabrication of α-Fe_2O_3 thin films in order to attain the maximum SERS enhancement.

2 Experimental

2.1 Materials and instruments

HDI was purchased from Fluka, and methanol (HPLC grade) was supplied from Fisher. 4-Mercaptopyridine (4-Mpy) and 2-mercaptobenzothiazole (2-MBT) were bought from Aldrich. The other reagents were obtained from Sinopharm Chemical Reagent Co., Ltd. All water was distilled through Millipore Milli-Q water purification system with a resistivity of 18.2 MΩ.

Raman spectra were recorded with a Renishaw Micro-Raman spectroscopy system. The excitation line at 514.5 nm provided by an Ar^+ laser was used. Raman scattering was detected with a Peltier cooled (−70°C) standard CCD array sensors (576 × 384 pixels). Specially adapted Research Grade Leica DMLM microscope allowing confocal measurements with 2 μm depth resolution was used. The data acquisition time used in the measurement of 4-Mpy was 25 s. X-ray diffraction (XRD) was carried out on Bruker D8 Advanced X-ray diffractometer with use of Cu Kα radiation (λ = 0.1542 nm). The morphologies of the prepared α-Fe_2O_3 NPs and α-Fe_2O_3 thin films were observed by TEM (JEM-2100, 200 kV) and SEM (LEO-1550, 5 kV), respectively.

2.2 Preparation of α-Fe_2O_3 NPs and suspension

100 nm α-Fe_2O_3 NPs (Sample 1) were prepared according to the reported method [24]. 3 mmol ferric chloride and 0.6 g cetyltrimethylammonium bromide (CTAB) was dissolved into water and kept stirring for 30 min. After that, the whole mixture was transferred into a Teflon-lined stainless steel autoclave, sealed, and maintained at 80°C for 10 h. Finally, it was heated to 180°C with a heating ramping of 1°C/min, and kept at the temperature for 12 h.

65 nm α-Fe_2O_3 NPs (Sample 2) were achieved according to the previously published procedure [25]. Concentrated (ms 37%) HCl was added to 100°C water to make a 0.002 mol/L HCl solution, and then 0.02 mol/L ferric chloride was dissolved in this hot solution. The temperature was kept at 100°C for 5 days.

5 nm α-Fe_2O_3 NPs (Sample 3) were obtained according to the following method. 0.05 mol ferric chloride and 0.15 mol sodium hydroxide was added into 250 mL water and kept stirring for 1 h, and reddish brown deposits were obtained. The deposits were rinsed and dried. After that, the deposits were diluted with 100 mL water to make 0.07 mol/L $Fe(OH)_3$ sol. 250 mL of n-butanol solution was injected into this sol, and then was heated to 190°C and refluxed for 24 h. At last, the dry powder was obtained by centrifuging the mixture and washing the sediment four times with 400 mL of water.

8.4 mg of the resulting α-Fe_2O_3 powder was dried under vacuum at 100°C for 2 h and then was dropped into 50 mL anhydrous toluene with ultrasonic agitation under nitrogen for 3 h. Then the homogeneous dispersed suspension of α-Fe_2O_3 was obtained.

2.3 Fabrication of α-Fe_2O_3 nanosensors

Figure 1 shows the fabrication strategy of α-Fe_2O_3 nanosensors [26]: At first, quartz slides (about 0.5 cm × 0.5 cm) were cleaned in H_2O_2/H_2SO_4 solution at 100°C for 10 min. Then they were rinsed with ethanol and water, and further dried under vacuum at 100°C for 2 h. In the second step, the above clean slides were submerged into a solution of 4 mL HDI in 40 mL anhydrous toluene at 60°C under nitrogen. After 24 h, the slides were rinsed with extensive anhydrous toluene to remove unbound HDI from the surface. In the final step, the slides were immerged into the suspension of α-Fe_2O_3, and heated at 60°C for 24 h. These substrates were rinsed profusely with methanol and dried under vacuum at 60°C for 2 h.

2.4 Preparation of the sample for Raman measurement

To record the Raman spectrum of 4-Mpy and 2-MBT adsorbed on α-Fe_2O_3 thin films, the substrates were immersed into 10 mL 10^{-6} mol/L 4-Mpy and 2-MBT methanol solution, respectively. After 24 h, the sample was removed and measured.

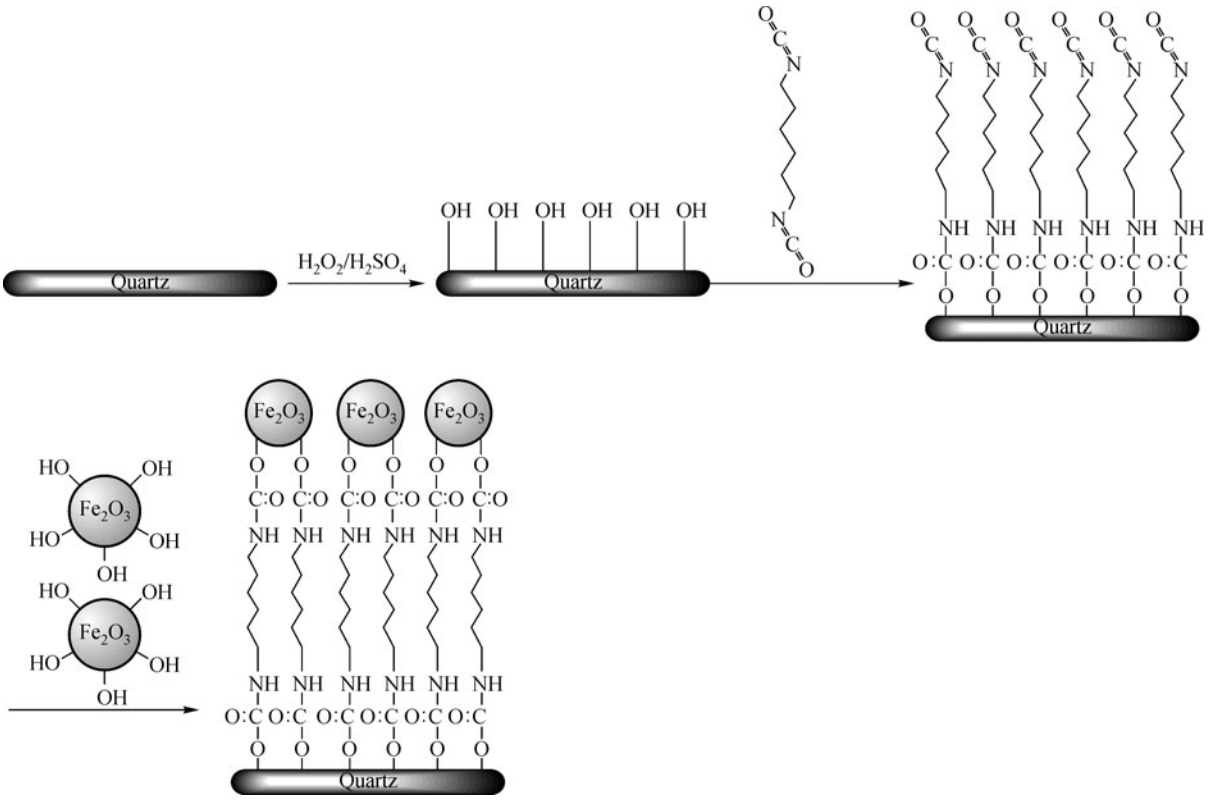

Figure 1 Schematic of the fabrication process for α-Fe_2O_3 thin films assembly

3 Results and discussion

3.1 Characterization of α-Fe_2O_3 nanosensors

X-ray diffraction patterns of the obtained three sized α-Fe_2O_3 particles are shown in Fig. 2. They have the same diffraction peaks appearing at about 24.4°, 33.3°, 35.8°, 41.1°, 49.9°, 54.2°, 57.8°, 62.6° and 64.2°, corresponding to the characteristic planes of (012), (104), (110), (113), (024), (116), (018), (214) and (300), which reveal the presence of α-Fe_2O_3 only. The TEM images of α-Fe_2O_3 NPs are shown in Fig. 3. As shown in Figs. 3(a–c), the samples 1, 2 and 3 present the relatively similar distribution with the respective average diameters of ca. 100, 65 and 5 nm. And the SEM images of the corresponding substrates are presented in Fig. 4, which show that α-Fe_2O_3 NPs distribute on the substrates in sub-monolayer mode on the whole, although the particles of Sample 3 is too small to discern. These images verify the strategy depicted by Fig. 1 that the α-Fe_2O_3 NPs were coated firmly on the modified surface. The classical electromagnetic enhancement mechanism on metals is usually considered that the very strong enhancements observed on the metal surfaces are usually obtained from particular sites, the so-called "hot spots", which may be junctions and interstices between metal

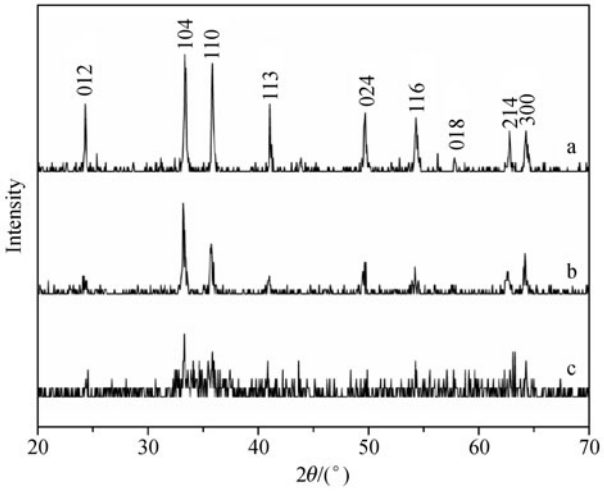

Figure 2 X-ray diffraction patterns of the resulting α-Fe_2O_3 particles: (a) 100 nm; (b) 65 nm; (c) 5 nm

nanoparticles [27,28]. It is known that when two nanoparticles approach each other, their transition dipoles get coupled, and the electromagnetic field around each nanoparticle is enhanced greatly. However, the rise of this huge enhancement (10^6 through 10^{14}) is still at dispute. Researchers constructed several SERS-active substrates to systematically study the

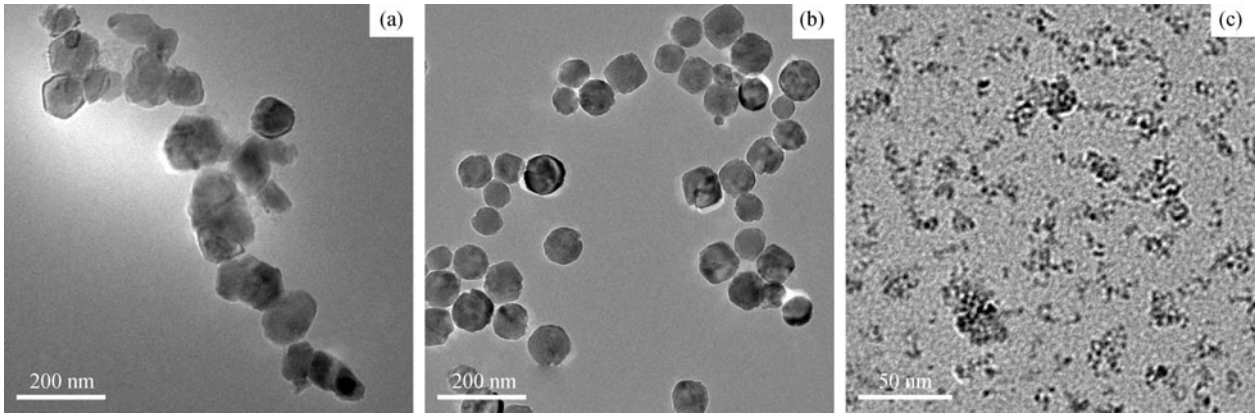

Figure 3 TEM micrographs of α-Fe_2O_3 particles: (a) 100 nm; (b) 65 nm; (c) 5 nm

enhancement mechanism or the hot spots. What is the most attractive is the highly ordered array structures composed by highly ordered nanoparticles because of their properties of uniform roughness, high sensitivity, long time stability and high concentration of hot spots. Among these highly ordered nanostructures, thin film is the alternative one. However, for most semiconductors, the plasmon resonance is typically in the infrared [29]. This value is too far away from the 514 nm incident light to be responsible for the observed enhancement in α-Fe_2O_3. Therefore, surface plasmon resonances may not be responsible for the observed enhancement in α-Fe_2O_3.

Until now, for most semiconductors, including α-Fe_2O_3, the Raman enhancement mechanism has not been clear. Lombardi group [30] did lots of work on the mechanism of SERS. They figured out that the enhancement stems from three sources: One is the surface plasmon resonance caused by the interaction of light with a metal nanoparticle, or more importantly, a cluster of nanoparticles. The second is a charge-transfer resonance between an adsorbed molecule and the metal conduction band. The third resonance occurs when one of the molecule resonance lies near the excitation frequency, and can greatly increase the observed enhancement factor. Usually, at a single excitation wavelength, it is often difficult to distinguish the degree to which each of the types of resonance contributes to the overall enhancement. At semiconductors system, their experiments further suggest that charge-transfer plays the predominant contribution on the enhancements. In this article, we consider that charge-transfer enhancement is most responsible for the observed enhancement, whereas the highly ordered structures play a synergistic role.

3.2 SERS spectra of 4-Mpy adsorbed on α-Fe_2O_3 thin films

Figures 5(a–c) show the SERS spectra of 4-Mpy on the surface of thin films with different α-Fe_2O_3 particle sizes. The intensities of Raman bands from 4-Mpy on Sample 2 are almost twice that of Sample 3, and the enhancement can be observed in the order of Samples $2 > 1 > 3$. Finkelstein-Shapiro et al. [31] have displayed that the SERS enhancement effects also depend on the nanoparticles size. It indicates that the α-Fe_2O_3 NPs have an optimum enhancement size. In addition, the SERS bands of 4-Mpy on Sample 1 are narrower than Samples 2 and 3.

For comparison, a normal Raman spectrum of bulk 4-Mpy is obtained under identical experimental conditions, as well as

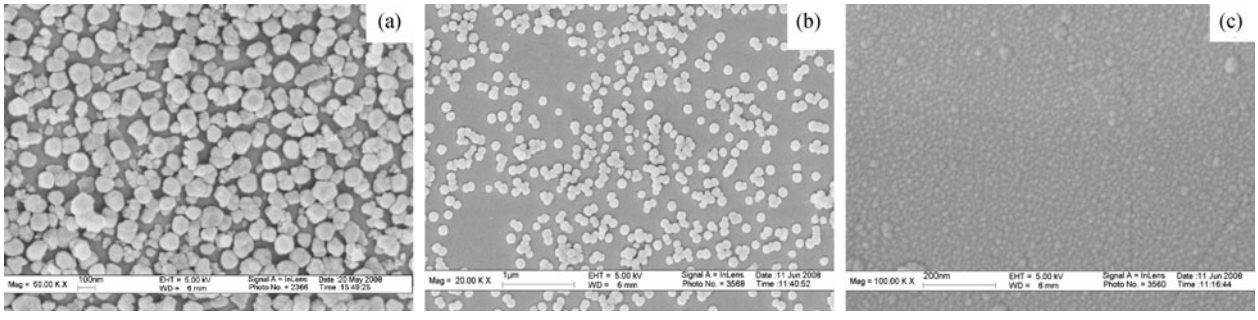

Figure 4 SEM micrographs of α-Fe_2O_3 nanoparticle thin films with samples of different sizes: (a) 100 nm; (b) 65 nm; (c) 5 nm

the Raman spectrum of the adsorbate-free surface (Fig. 5). The corresponding band assignments are listed in Table 1. In the absence of adsorbate, no major peaks are observed in the Raman spectrum, indicating that SERS from the adsorbate-free surface is very weak. It is observed that the S-H stretching at approximate 2570 cm^{-1} in the normal Raman spectrum is completely missing in the SERS spectrum (not shown). Since 4-Mpy exists in the thiol-thione tautomer, the disappearance of this band is not a reliable evidence to confirm the rupture of the SH bonding [22,32]. Nevertheless, the appearance of the strong enhanced band at 1150 cm^{-1} corresponds to the ring-breathing / C–S stretching mode, which indicates that 4-Mpy is adsorbed on α-Fe_2O_3 thin films surface through the sulfur atom. It is also supported by the C–S stretching mode at 713 cm^{-1}, which displays an increase in intensity.

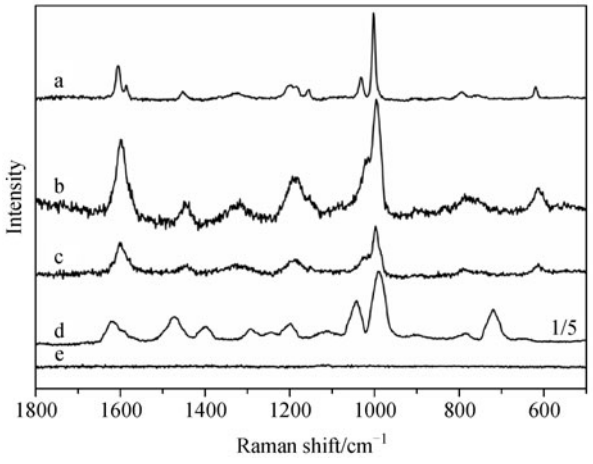

Figure 5 SERS spectra of 4-Mpy adsorbed on α-Fe_2O_3 thin films with different size samples: (a) 100 nm; (b) 65 nm; (c) 5 nm; (d) normal Raman spectrum of bulk 4-Mpy; (e) Raman spectrum of the adsorbate-free surface

Table 1 Raman frequencies (cm^{-1}) and band assignments for 4-Mpy

Bulk	SERS	Assigment[a)]
1616	1598	*ν*CC
1594	1579	*ν*CC
1471	1450	*ν*CC / *ν*CN
1397		*ν*CC
1293	1321	*β*CH
1243		*β*CH
1199	1189	*β*CH / *δ*NH
1110	1150	ring-breathing / *ν*CS
1044	1021	*β*CH
991	997	ring-breathing
903	907	*γ*CH
785	787	*γ*CH
720	713	*β*CC / *ν*CS
644	616	*β*CCC

a) Assignment for 4-Mpy from Refs. [22,32].

In order to understand the orbital nature of the charge-transfer process, we take advantage of the considerable literature on photo-dissociation dynamics of thiophenol [33,34]. In these work, Kim and coworkers explore the molecular orbital nature of the photo-dissociation of thiophenol to phenylthiyl radical. Since most of the low-lying transitions involved p-orbitals on the S atom, their results should be applicable to charge-transfer in adsorbed 4-Mpy as well, since the only difference is that the pyridine ring is replaced by a benzene ring. It is likely that the 4-Mpy is attached to the thin film surface through S atom bonding to a partially positive Fe atom on the surface. This is facilitated by the removal of the thiol H atom, so that the most likely adduct is 4-pyridylthiyl radical. Charge-transfer from α-Fe_2O_3 valence band will then take place in the lowest p-orbitals on the S atom.

It should be noted that the enhanced bands (1598, 1579, 1450, 1321, 1189, 1150, 1021, 997, 787, 616 cm^{-1}) in the SERS spectrum are all attributed to in-plane vibration modes. According to the SERS selection rules [35,36], these in-plane vibration modes in the SERS of 4-Mpy suggest the perpendicular orientation of 4-Mpy molecules to the surface of α-Fe_2O_3 thin films [37,38]. Therefore, 4-Mpy molecules adsorbed onto the surface of α-Fe_2O_3 thin films through the sulfur atom at a perpendicular orientation.

In addition, the SERS spectra of 2-MBT adsorbed on α-Fe_2O_3 thin films are also recorded in Fig. 6, in which it is clear that the Raman signals of 2-MBT adsorbed on α-Fe_2O_3 thin films are enhanced. In Figs. 6(a–c), the ring-breathing /*ν*CS vibrational mode at 1151 cm^{-1} exhibits a great enhancement compared with that in Raman spectrum of bulk 2-MBT.

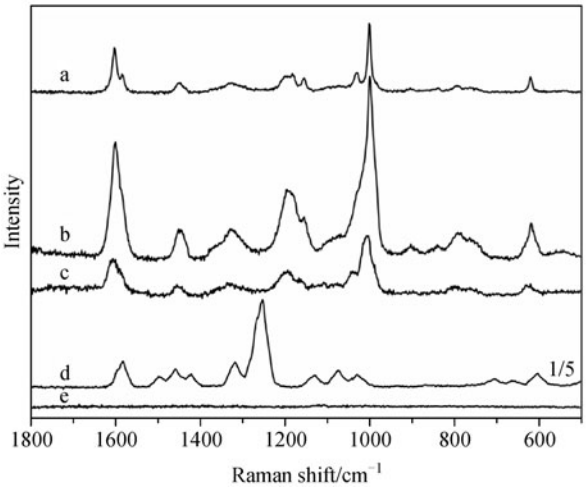

Figure 6 SERS spectra of 2-MBT adsorbed on α-Fe_2O_3 thin films with different size samples: (a) Sample 1, (b) Sample 2, (c) Sample 3; (d) normal Raman spectrum of bulk 2-MBT; (e) Raman spectrum of the adsorbate-free surface

Besides, the C–S stretching mode at 619 cm^{-1} is also observed in the SERS spectrum of 2-MBT on the surface of α-Fe_2O_3 thin films. Therefore, similar to 4-Mpy, 2-MBT adsorbed onto the surface of α-Fe_2O_3 thin films through the sulfur atom.

3.3 Estimation for the efficiency of α-Fe_2O_3 nanosensors

The SERS spectra from 4-Mpy at different concentrations adsorbed on the surface of α-Fe_2O_3 thin film (Sample 2) are shown in Fig. 7. When the concentrations of 4-Mpy change from 10^{-5} to 10^{-8} mol/L, the intensities of peaks are almost the same, but they get weakened when the concentration decreases to 10^{-9} mol/L. It indicates that the saturated adsorption concentration of 4-Mpy on the α-Fe_2O_3 thin films surface is 1×10^{-8} mol/L. Note that even though the concentration decreases to 10^{-12} mol/L, it remains possible to detect the Raman signal of the adsorbed 4-Mpy molecules.

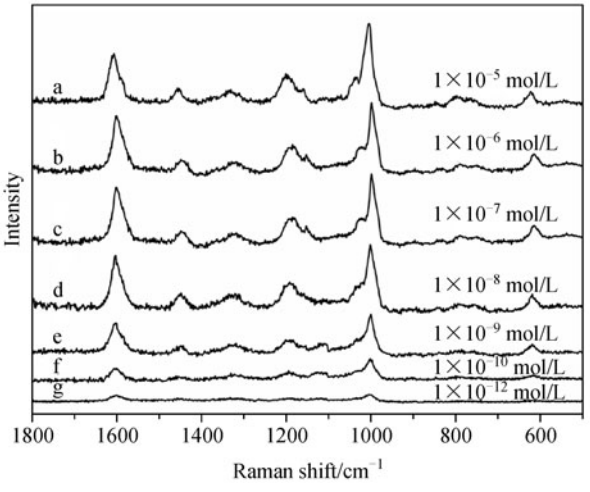

Figure 7 SERS spectra from 4-Mpy at different concentrations adsorbed on the surface of α-Fe_2O_3 thin films: (a) 1×10^{-5} mol/L; (b) 1×10^{-6} mol/L; (c) 1×10^{-7} mol/L; (d) 1×10^{-8} mol/L; (e) 1×10^{-9} mol/L; (f) 1×10^{-10} mol/L; (g) 1×10^{-12} mol/L

To further evaluate the enhancement efficiency of this system, we quote a simple formula [39,40], $EF = (I_{SERS} / I_{bulk}) \times (N_{bulk} / N_{SERS})$, to estimate the enhancement factor (EF). I_{SERS} and I_{bulk} are Raman intensities of 4-Mpy adsorbed on α-Fe_2O_3 thin film (Sample 2) and 0.2 mol/L 4-Mpy solution, respectively, whereas N_{SERS} and N_{bulk} are the corresponding number of samples. When we choose the representative band at 1598 cm^{-1} as the typical band, the ratio of the intensities (I_{SERS} / I_{bulk}) is about 0.75. Taking the sample area (ca. 1 μm in diameter) of the laser beam into account, the calculated N_{bulk} / N_{SERS} is about 1.26×10^4. Therefore, the EF is estimated to be about 10^4.

4 Conclusion

Novel SERS-active nonmetallic nanosensors (α-Fe_2O_3 thin films) have been developed, which are capable of detecting probes at sub-micromolar ($< 10^{-6}$ mol/L), even at nanomolar (10^{-9} mol/L) concentration. During the fabrication process of α-Fe_2O_3 thin films, the cross-linker (HDI) plays important roles in fabricating uniformly roughed, stable and immobilized surface. The morphology-specific surface results in large Raman enhancements from probe molecules. Furthermore, by regulating the particle size, we found that α-Fe_2O_3 NPs have an optimum enhancement size nearby 65 nm. Charge-transfer enhancement is the most responsible for the observed enhancement, and the highly ordered structures play a synergistic role.

Acknowledgements This work was supported by the Natural Science Foundation of Jiangsu Higher Education Institutions of China (No. 09KJD150002), Zhenjiang Science and Technology Bureau (No. GJ2006006) and Jiangsu University High-grade Specialty Person Scientific Research Foundation (No. 10JDG114).

References

1. Wang, Y.; Li, D.; Li, P.; Wang, W.; Ren, W.; Dong, S.; Wang, E., *J. Phys. Chem. C* **2007**, *111*, 16833–16839
2. Sylvia, J. M.; Janni, J. A.; Klein, J. D.; Spencer, K. M., *Anal. Chem*. **2000**, *72*, 5834–5840
3. Yonzon, C. R.; Stuart, D. A.; Zhang, X.; McFarland, A. D.; Haynes, C. L.; Van Duyne, R. P., *Talanta* **2005**, *67*, 438–448
4. Lucotti, A.; Pesapane, A.; Zerbi, G., *Appl. Spectrosc*. **2007**, *61*, 260–268
5. Wachter, E. A.; Storey, J. M. E.; Sharp, S. L.; Carron, K. T.; Jiang, Y., *Appl. Spectrosc*. **1995**, *49*, 193–199
6. Grabar, K. C.; Freeman, R. C.; Hommer, M. B.; Natan, M. J., *Anal. Chem*. **1995**, *67*, 735–743
7. Krenn, J. R.; Hohenau, A.; Leitner, A.; Aussenegg, F. R., *J. Chem. Phys*. **2004**, *120*, 15
8. Freeman, R. G.; Grabar, K. C.; Allison, K. J.; Bright, R. M.; Davis, J. A.; Guthrie, A. P.; Hommer, M. B.; Jackson, M. A.; Smith, P. C.; Walter, D. G.; Natan, M. J., *Science* **1995**, *267*, 1629–1632
9. Chumanov, G.; Sokolov, K.; Gregory, B. W.; Cotton, T. M., *J. Phys. Chem*. **1995**, *99*, 9466–9471
10. Ulman, A., *Chem. Rev*. **1996**, *96*, 1533–1554
11. Murty, K. V. G. K.; Venkataramanan, M.; Pradeep, T., *Langmuir* **1998**, *14*, 5446–5456
12. Felidj, N.; Truong, S. L.; Aubard, J.; Levi, G.; Krenn, J. R.; Hohenau, A.; Leitner, A.; Aussenegg, F. R., *J. Chem. Phys*. **2004**, *120*, 7141
13. Tantra, R.; Brown, R. J. C.; Milton, M. J. T.; Gohil, D., *Appl. Spectrosc*. **2008**, *62*, 992–1000
14. Wang, Y.; Gan, L.; Chen, H.; Dong, S.; Wang, J., *J. Phys. Chem.*

B **2006**, *110*, 20418–20425
15. Zou, S.; Weaver, M. J., *Anal. Chem*. **1998**, *70*, 2387–2395
16. Brankovic, S. R.; Wang, J. X.; Adzic, R. R., *Surf. Sci*. **2001**, *474*, L173–L179
17. Wang, Z. L., *Adv. Mater. (Deerfield Beach Fla.)* **2003**, *15*, 432–436
18. Liu, A., *Biosens. Bioelectron*. **2008**, *24*, 167–177
19. Yamada, H.; Yamamoto, Y., *Surf. Sci*. **1983**, *134*, 71–90
20. Loo, B. H., *J. Electroanal. Chem*. **1982**, *136*, 209–213
21. Kudelski, A.; Grochala, W.; Janik-Czachor, M.; Bukowska, J.; Szummer, A.; Dolata, M., *J. Raman Spectrosc*. **1998**, *29*, 431–435
22. Fu, X.; Pan, Y.; Wang, X.; Lombardi, J. R., *J. Chem. Phys*. **2011**, *134*, 024707
23. Liu, Y. C.; Yu, C. C.; Wang, C. C.; Juang, L. C., *Chem. Phys. Lett*. **2006**, *420*, 245–249
24. Wang, X.; Chen, X.; Ma, X.; Zheng, H.; Ji, M.; Zhang, Z., *Chem. Phys. Lett*. **2004**, *384*, 391–393
25. Matijevic, E.; Scheiner, P., *J. Colloid Interface Sci*. **1978**, *63*, 509–524
26. Fu, X. Q.; Bei, F. L.; Wang, X.; Yang, X. J.; Lu, L. D., *J. Raman Spectrosc*. **2009**, *40*, 1290–1295
27. Su, X.; Zhang, J.; Sun, L.; Koo, T. W.; Chan, S.; Sundararajan, N.; Yamakawa, M.; Berlin, A. A., *Nano Lett*. **2005**, *5*, 49–54
28. Lee, S. J.; Morrill, A. R.; Moskovits, M., *J. Am. Chem. Soc*. **2006**, *128*, 2200–2201
29. Wang, Y.; Zhang, J.; Jia, H.; Li, M.; Zeng, J.; Yang, B.; Zhao, B.; Xu, W.; Lombardi, J. R., *J. Phys. Chem. C* **2008**, *112*, 996–1000
30. Lombardi, J. R.; Birke, R. L. J., *PhysChemComm* **2008**, *112*, 5605
31. Finkelstein-Shapiro, D.; Tarakeshwar, P.; Rajh, T.; Mujica, V., *J. Phys. Chem. B* **2010**, *114*, 14642–14645
32. Baldwin, J. A.; Vlckova, B.; Andrews, M. P.; Butler, I. S., *Langmuir* **1997**, *13*, 3744–3751
33. Lim, J. S.; Choi, H.; Lim, I. S.; Park, S. B.; Lee, Y. S.; Kim, S. K., *J. Phys. Chem. A* **2009**, *113*, 10410–10416
34. Lim, I. S.; Lim, J. S.; Lee, Y. S.; Kim, S. K., *J. Chem. Phys*. **2007**, *126*, 034306
35. Moskovits, M., *Rev. Mod. Phys*. **1985**, *57*, 783–826
36. Moskovits, M., *J. Chem. Phys*. **1982**, *77*, 4408
37. Kalkar, A. K.; Bhossekar, N. M.; Kshirsagar, S. T., *Spectrochim. Acta [A]* **1989**, *45A*, 635–641
38. Muniz-Miranda, M.; Neto, N.; Sbrana, G., *J. Phys. Chem*. **1988**, *92*, 954–959
39. Wang, Y. F.; Sun, Z. H.; Hu, H. L.; Jing, S. Y.; Zhao, B.; Xu, W. Q.; Zhao, C.; Lombardi, J. R., *J. Raman Spectrosc*. **2007**, *38*, 34–38
40. Park, H. K.; Yoon, J. K.; Kim, K., *Langmuir* **2006**, *22*, 1626–1629